

Article

Enhanced Photocatalytic Activity of rGO-CuO Nanocomposites for the Degradation of Organic Pollutants

Suresh Sagadevan ^{1,*}, Jayasingh Anita Lett ², Getu Kassegn Weldegebrail ³ , Seema Garg ⁴ , Won-Chun Oh ^{5,*}, Nor Aliya Hamizi ¹ and Mohd Rafie Johan ¹

- ¹ Nanotechnology & Catalysis Research Centre, University of Malaya, Kuala Lumpur 50603, Malaysia; aliyahamizi@um.edu.my (N.A.H.); mrafiej@um.edu.my (M.R.J.)
- ² Department of Physics, Sathyabama Institute of Science and Technology, Chennai 600119, Tamil Nadu, India; janitalett17@gmail.com
- ³ Department of Chemistry, College of Natural and Computational Sciences, Debre Berhan University, Debre Berhan P.O. Box 445, Ethiopia; belay.kassegn@gmail.com
- ⁴ Department of Chemistry, Amity Institute of Applied Sciences, Amity University, Sector-125, Noida 201313, Uttar Pradesh, India; sgarg2@amity.edu
- ⁵ Department of Advanced Materials Science and Engineering, Hanseo University, Seosan-si 356-706, Chungnam, Korea
- * Correspondence: drsureshsagadevan@um.edu.my (S.S.); wc_oh@hanseo.ac.kr (W.-C.O.)

Abstract: Copper oxide (CuO) nanoparticles (NPs) were decorated on reduced graphene oxide (rGO) through the effective synthetic route method. Powder X-ray diffraction, Fourier transform infrared, ultraviolet-visible absorption, and scanning electron microscopy techniques were used to analyze the chemical structure, functional groups, absorbance, and morphology. Under visible light illumination, the CuO/rGO nanocomposites have higher catalytic activity compared to the bare CuO NPs which were suitable for degradation of methylene blue (MB) and Congo red (CR) dyes. According to the findings, the CuO/rGO nanocomposites possess excellent photocatalytic efficiency. Thus, the synthesized CuO/rGO nanocomposite is a promising photocatalyst for the deterioration of organic pollutants in water and wastewater treatment.

Keywords: reduced graphene oxide; CuO; methylene blue (MB); Congo red (CR); photocatalytic degradation



Citation: Sagadevan, S.; Lett, J.A.; Weldegebrail, G.K.; Garg, S.; Oh, W.-C.; Hamizi, N.A.; Johan, M.R. Enhanced Photocatalytic Activity of rGO-CuO Nanocomposites for the Degradation of Organic Pollutants. *Catalysts* **2021**, *11*, 1008. <https://doi.org/10.3390/catal11081008>

Academic Editor: Javier Ereña Loizaga

Received: 7 August 2021

Accepted: 19 August 2021

Published: 21 August 2021

Publisher's Note: MDPI stays neutral with regard to jurisdictional claims in published maps and institutional affiliations.



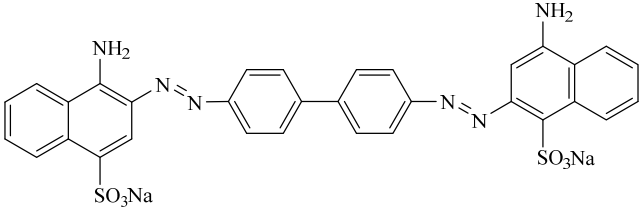
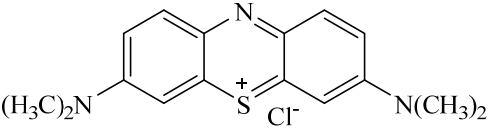
Copyright: © 2021 by the authors. Licensee MDPI, Basel, Switzerland. This article is an open access article distributed under the terms and conditions of the Creative Commons Attribution (CC BY) license (<https://creativecommons.org/licenses/by/4.0/>).

1. Introduction

Copper oxides have received a lot of consideration due to their special properties such as stability, suitability for the environment, low production cost, and abundant availability. They have been incorporated in many practical uses such as in solar cells, photocatalysts, and gas sensor applications [1–4]. Due to their cheap cost, high oxidizing characteristics and lack of toxicity, TiO₂ and ZnO-based catalysts are frequently utilized in photocatalytic applications to remove organic contaminants from water [5–7]. The photocatalytic efficacy of catalysts is low, due to the large bandgap (>3.2 eV), necessitating significant UV absorption energy. Copper (II) oxide or cupric oxide (CuO) is a well-known intrinsically p-type semiconductor with a bandgap of 1.2 eV [8–10]. In the photocatalytic process, this can be a significant benefit over broad bandgap for the semiconducting materials, as sunlight can be fully exploited. Despite this, the photocatalytic efficacy of copper oxide is poor due to the extraordinarily high recombination rate of the photogenerated electron hole (e^-/h^+) pairs. As a result, by mixing electron-accepting materials with copper oxide, the recombination of e^-/h^+ pairs must be reduced. Due to the exceptional thermal and mechanical stability, great surface area, and ease of surface modification, graphene has recently gained a lot of attention as a supporting material [11,12]. The advantages of loading copper oxide on graphene would be used to increase photocatalytic efficacy. Though graphene-based copper oxide is a promising option for a photocatalyst, only a few examples are available

in photocatalytic applications, and the full structural characterization of CuO-graphene has yet to be published [13–16]. This study tested CuO/rGO nanocomposites in the photocatalytic activities of two organic dyes, methylene blue (MB) and Congo red (CR), under visible light irradiation. While MB is cationic thiazine dye, CR is anionic azo dye, containing the azo (-N=N-) functional group in its structure. Both dyes are extensively used in the textile industry and could cause health problems if they are discharged to the environment without prior treatment. Table 1 provides the structural formula and toxicity of these dyes.

Table 1. Structural formula, maximum UV-vis absorption (λ_{max}), and toxicity of CR and MB dyes.

Dye	The Structural Formula (Molecular Mass (g/mol), Ionicity)	λ_{max} (nm)	Toxicity	Ref.
CR	 <p>(696.7, anionic)</p>	497	Carcinogenic and mutagenic	[17]
MB	 <p>(373.9, cationic)</p>	664	Anemia, jaundice, dizziness, tissue necrosis, gastrointestinal problems, eye problem in humans	[18,19]

The main aim of this work is to (a) develop a simple and easy way to synthesize CuO/rGO nanocomposites, (b) examine its morphological and chemical structures using Powder X-ray diffraction (XRD), Fourier transform infrared (FTIR) scanning electron microscopy (SEM) and Energy Dispersive X-Ray Analysis (EDAX) techniques, and (c) assess and compare their photocatalytic degradation efficiency for MB and CR dyes and learn about the link between structural characteristics and photocatalytic performance.

2. Results and Discussion

2.1. Physicochemical Properties

Figure 1 depicts copper oxide (CuO) development on reduced graphene oxide (rGO) using XRD analysis. GO exhibits a distinct XRD diffraction peak centered at 42.6° . The inclusion of various oxygen functional groups (hydroxyl, epoxy, carbonyl groups, etc.) on either side of the graphene layers has credited to the peak at 10.9° , whereas the peak at 42.6° corresponds to the (100) plane of the hexagonal structure of carbon [20,21]. Additional diffraction peaks arise at $2\theta = 35.6^\circ$ and 38.8° when the copper-precursor impregnates GO, which can be connected with the (111) and (111) planes of the monoclinic structured CuO [13,22]. Figure 1 displays an XRD pattern of CuO/rGO in which the diffraction peaks are closely aligned with the monoclinic phase of CuO. Monoclinic structured CuO peaks corresponding to the planes (110), (111), (111), (202), (020), (202), and (311) are well-matched with the standard diffraction peaks (JCPDS 48-1548) [21–24]. The crystallite size (D) was calculated to be in the range of 45–50 nm for the prepared rGO/CuO nanocomposites using Scherrer formula given by $D = \kappa\lambda / \beta \cos\theta$ from the XRD most intense peak.

Here, k is a constant equal to 0.9, λ is the wavelength of X-ray radiation ($\lambda = 0.15406$ nm), β represents the peak width at half maximum intensity of the peak selected, and θ is the Bragg's angle.

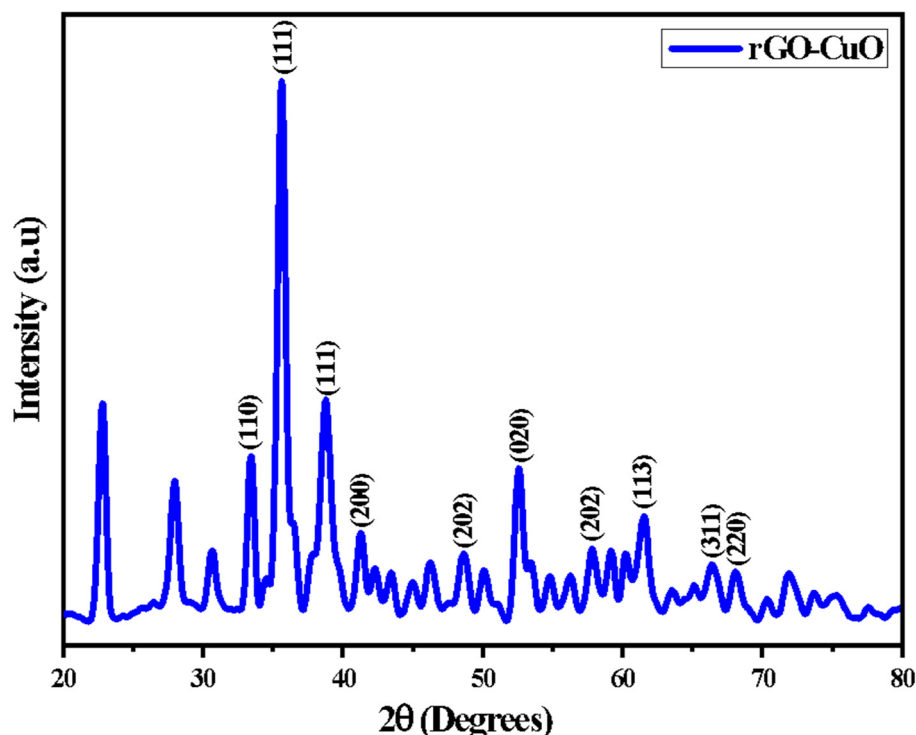


Figure 1. XRD pattern of as-synthesized rGO-CuO nanocomposites.

Figure 2a–d depicts the surface morphology and chemical composition of rGO/CuO nanocomposites. From the analysis of SEM images for rGO/CuO nanocomposite, the nanostructure is found to be in the form of flakes due to the presence of GO. This decoration of CuO on GO occurs due to the enhanced interfaces between CuO and the functional group existing in the molecular mixing phase on the GO surface [25]. The EDAX analysis shows the elemental mapping of the rGO-CuO nanocomposite, along with FESEM, and the generated results are given in Figure 3. It defines that the elemental mapping of the rGO-CuO sample has 39% Cu, 49% O, and 12% C. This confirms the occurrence of rGO in the rGO-CuO sample, i.e., the CuO particles are uniformly distributed onto the graphene layers. Additionally, it can be observed that the amount of C is very low (therefore it could not be detected in the XRD) and this shows the decrease in the C distribution in the nanocomposite. It is partially due to the quenching of the GO to graphene. From the overall analysis of FESEM, EDAX, and EDS, the rGO-CuO nanocomposites are successfully synthesized without any impurities.

FTIR spectroscopy helps in identifying the existence of the vibrational frequencies in the synthesized rGO/CuO nanocomposite as shown in Figure 4. The peak at 1117 cm^{-1} attributes to C–O stretching vibrations, and the characteristic peak at 1566 cm^{-1} shows the presence of C=C in a graphene oxide sheet [26]. The wavenumber at 3389 cm^{-1} corresponds to O–H stretching vibration, which gets significantly reduced in the rGO [27]. The peak at 882 cm^{-1} is due to the Cu–OH vibration, confirming the effective preparation of the rGO/CuO nanocomposite [28]. The absorption peak at 432 cm^{-1} corresponds to Cu–O stretching vibrations denoting that CuO has completely decorated on the rGO sheet [25].

UV–vis absorption spectrum has been recorded for the prepared rGO-CuO nanocomposites and is shown in Figure 5. The rGO-CuO nanocomposites correspond to $n\text{--}\pi^*$ and $\pi\text{--}\pi^*$ transitions, and these transitions are due to the presence of aromatic carbon–carbon bond and carbonyl group [29]. The absorption spectrum indicates the reduction in GO and the replacement of the OH and COOH group with CuO. The absorption peak at 300 nm shows the complete disappearance and confirms the reduction in GO and the fixing of CuO on the GO sheet [30,31].

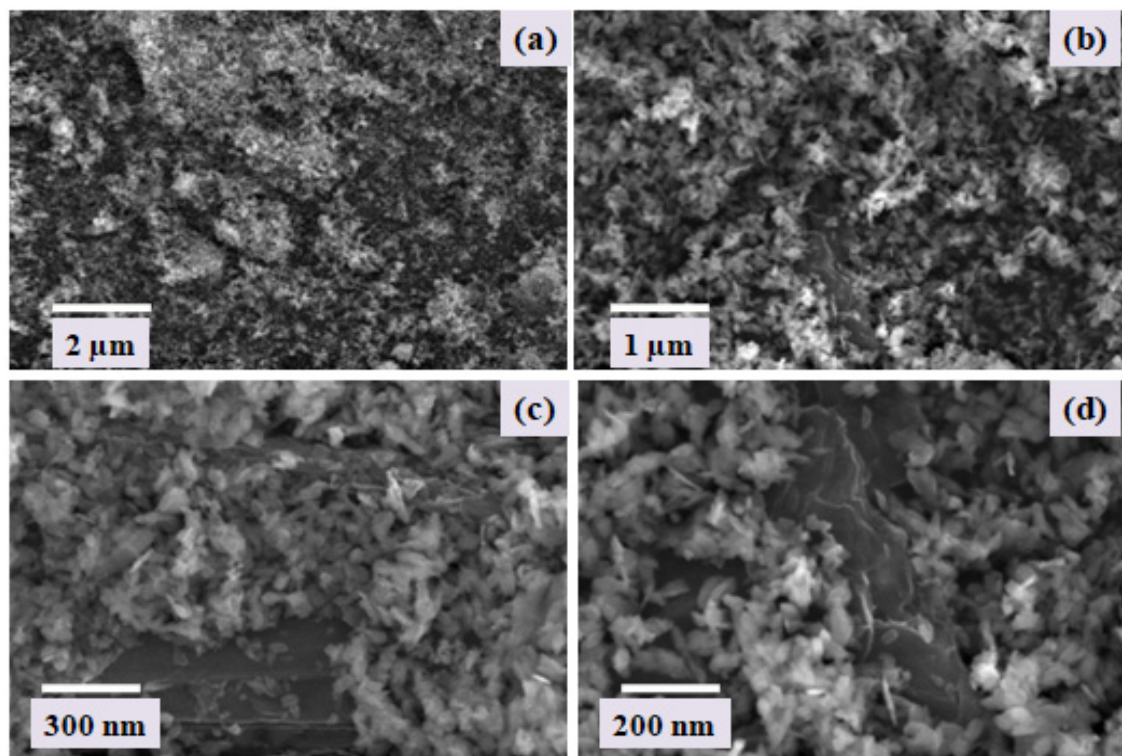


Figure 2. FESEM images of (a–d) rGO-CuO nanocomposites with different magnifications.

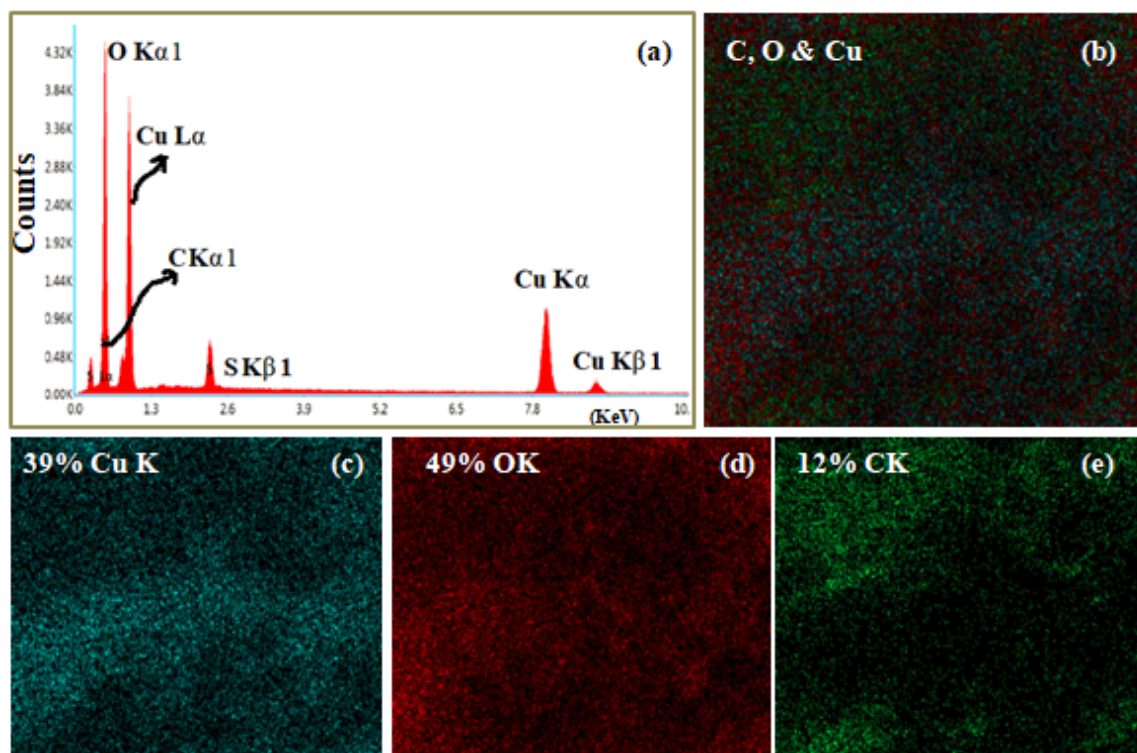


Figure 3. (a) EDAX analysis and (b–e) EDS mapping of the synthesized rGO-CuO composite.

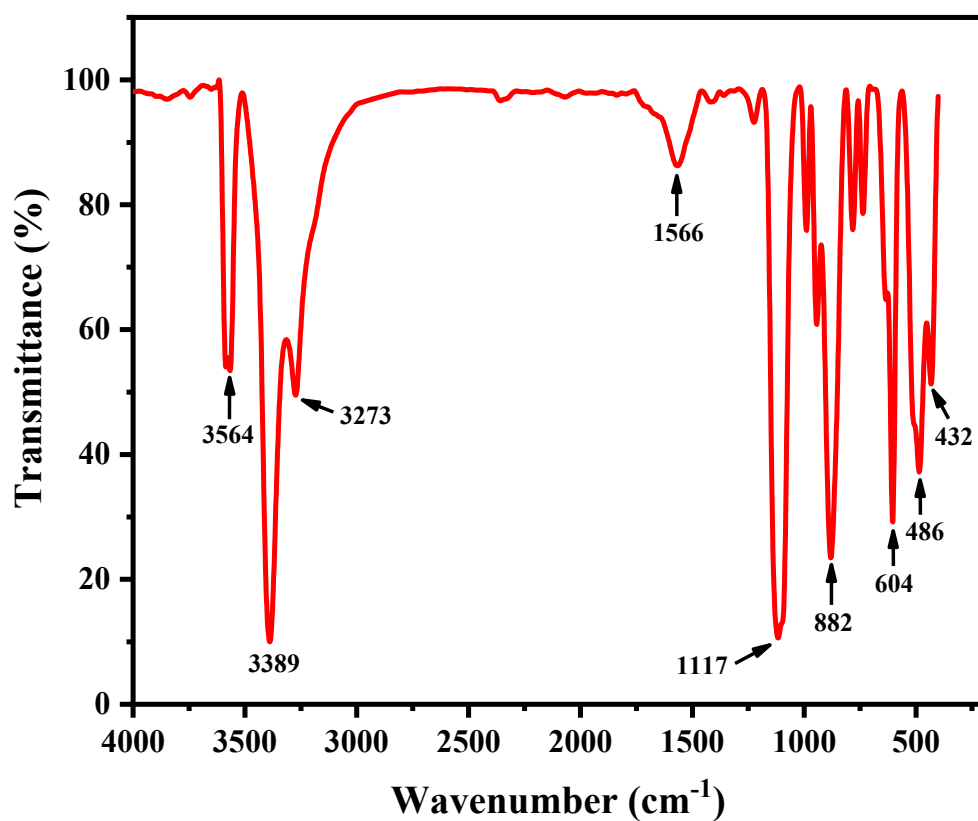


Figure 4. FTIR spectrum of the synthesized rGO-CuO nanocomposites.

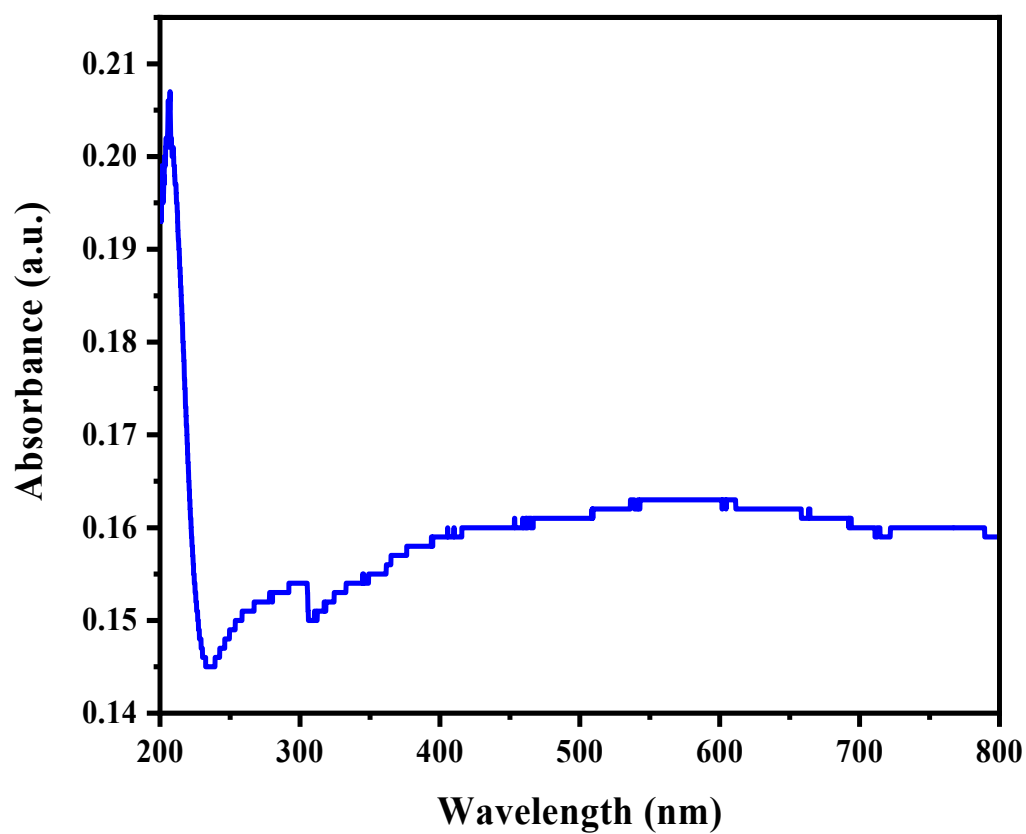


Figure 5. UV-vis absorption spectrum of rGO-CuO nanocomposites.

2.2. Photocatalytic Activity of CuO/rGO Nanocomposites

The photocatalytic activity of CuO/rGO composites was tested for MB and CR dyes, and it can be seen from Figure 6 that the hypochromic shift in absorbance with time for both dyes imply their degradation in a period of 1 h, Figure 6a,b. As shown in Figure 6c,d, the resulting percent of degradation (D (%)), given by Equation (1), is achieved as 95.6% for CR and 77.5% for MB under visible light illumination for 1 h.

$$D (\%) = \left(1 - \frac{A_t}{A_0}\right) \times 100 \quad (1)$$

where, A_0 and A_t represent the initial absorbance before radiation exposure and after exposure time t , respectively.

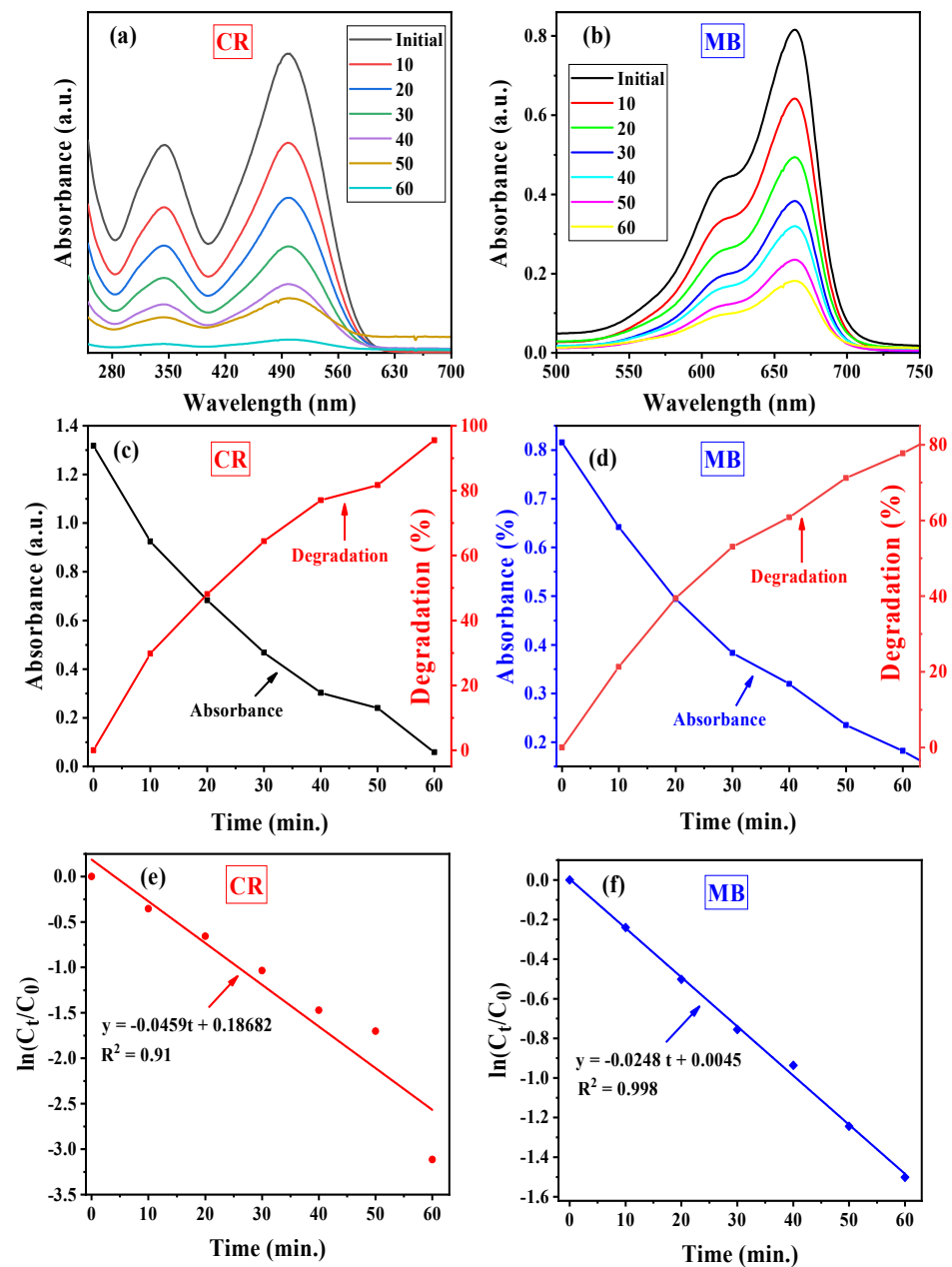


Figure 6. Decrease in absorption intensity with time (a,b), absorbance and degradation percentage (c,d) and kinetics plots (e,f) for the degradation of CR and MB dyes, respectively, in 1 h of irradiation under visible light utilizing rGO-CuO nanocomposites as a catalyst.

Moreover, the experimental degradation reactions can be described with satisfactory values of correlation coefficients (R^2), Figure 6e,f using pseudo-first-order reaction rate constant (k_{app}), Equation (2). From the plots, the respective reaction rate constants for the degradation of CR and MB dyes are 0.0459 and 0.0248 min^{-1} as tabulated in Table 2.

$$\ln \left(\frac{C_t}{C_0} \right) = -k_{app}t \quad (2)$$

$$t_{1/2} = \frac{\ln(2)}{k_{app}} = \frac{0.693}{k_{app}} \quad (3)$$

Table 2. Summary of photocatalytic parameters for the degradation of CR and MB dyes using rGO/CuO nanocomposites.

S/N	Dye	D (%)	t (min.)	k_{app} (min.^{-1})	$t_{1/2}$ (min.)	R^2
1	CR	95.6	60	0.0459	15.1	0.91
2	MB	77.7	60	0.0248	27.9	0.998
3	MB	92.8	90	0.0275	25.2	0.98

The photocatalytic activity of pure CuO nanoparticles for the degradation of methylene blue was tested under similar experimental conditions. It was found that MB was decomposed by 26% under visible light irradiation for 1 h, a difference of about 52% as compared to the decomposition achieved using rGO-CuO as a photocatalyst. The similar enhanced photoactivity of rGO-CuO nanocomposites compared to the individual pure phases of CuO or rGO catalysts for the degradation of MB under visible light for 1 h was reported by Dutta et al. [27]. In their work, they found that MB was degraded by nearly 99% using the composites in the presence of H_2O_2 oxidant under visible light irradiation, which was superior to that achieved by the pure CuO or rGO phase catalysts, with their respective degradation percentages being 70 and 77% under similar experimental condition.

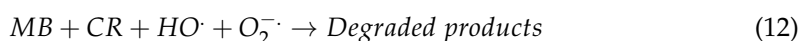
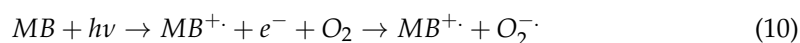
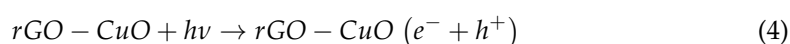
In another study, Kumar et al. [32] found an increase in photocatalytic activity of rGO/CuO nanocomposites for the degradation of MB under sunlight irradiation for 1 h by 10% as compared to the efficiency achieved by bare CuO NPs under similar experimental parameters. According to the authors, the enhanced activity of the rGO/CuO composites is due to the facilitated charge transfer created as a result of the synergistic effect between CuO crystal structures and π -conjugated structures in rGO, which prolong the recombination rate of charge carriers and increase the degradation rate.

Table 3 provides additional examples of reports for the degradation performance of rGO-CuO nanocomposites for different organic pollutants at the indicated experimental conditions. Therefore, the synthesized rGO-CuO composites are photoactive towards the degradation of MB and CR dyes. Photocatalytic degradation of dyes could occur via direct routes or indirect routes. In the direct route, decomposition occurs after photosensitization of the dyes by photon absorption and subsequent injection of photoexcited electrons into the conduction band of the semiconductor catalyst, reducing dissolved oxygen into superoxide radical ion (O_2^-) (Equations (9) and (10)), and then into more reactive hydroxyl radical ($\text{HO}\cdot$) through subsequent steps (Equations (7) and (8)). These two radicals are primary responsible for inducing the degradation reactions. In particular, the $\text{HO}\cdot$ Radical, with an oxidation potential of +2.8V vs. NHE, is the most powerful oxidizing radicals, which non-selectively degrades organic pollutant molecules via H abstraction, in addition to the unsaturated bond, and electron transfer mechanisms [33].

Table 3. Comparison of photocatalytic degradation performance of rGO-CuO nanocomposites for different organic pollutants with result in this work.

Catalyst	Pollutant	Conditions	D (%)	Ref.
CuO/rGO	2-Nitrophenol	2-Nitrophenol conc. = 10 ppm, catalyst dose = 30 mg, 400 W metal halide lamp, t = 3 h	100	[34]
rGO/CuO	4-Nitrophenol	4-Nitrophenol conc. = 0.253 ppm, catalyst dose = 10 mg, t = 240 min. under UV light	81	[35]
50%rGO/CuO	Methylene blue	MB conc. = 10 ppm, catalyst dose = 20 mg, 150 W Xe lamp, 20 mL H ₂ O ₂ added, t = 1 h	99	[27]
ZnO/rGO	Congo red	Congo red conc. = 10 ppm, Dye volume = 100 mL, catalyst dose = 50 mg, under visible light for 1 h	92	[36]
Cu/rGO	Methylene blue	Dye Conc. = 40 ppm, catalyst dose = 20 mg, t = 50 min.,	94	[37]
CuO-rGO	Methylene blue	MB conc. = 2.23×10^{-5} M, V = 50 mL, Catalyst dose = 10 mg using 100 W Xe lamp irradiating for 90 min.	77.7	Present work
	Congo red	CR conc. = 2.23×10^{-5} M, V = 50 mL, Catalyst dose = 10 mg using 100 W Xe lamp irradiating for 90 min.	95.6	

In the indirect route, decomposition is initiated by the in-situ generation of electron-hole pairs. When the semiconductor catalyst particles are irradiated with radiation of energy ($h\nu$), they are found to be (E_g), that is $h\nu \geq E_g$. After that, the CB electrons reduce electron-accepting species such as dissolved O_2 in solution to $O_2^{\cdot-}$, and VB holes cause the oxidation of electron-donating species such as H_2O into HO^{\cdot} radicals (Equations (5) and (6)). These then begin the decomposition process, producing intermediate steps initially, and finally converting them into environmentally benign products of CO_2 , H_2O , and few mineral acids (Equation (12)). Of the two possible decomposition routes, it has been found that the indirect route is kinetically faster, as well as the predominant route leading to the decomposition of organic pollutants [38]. The overall steps involved during the destruction process of the dyes are outlined in Equations (4)–(12).



In addition to the nature of the catalyst and its morphological properties, several operational parameters including initial pollutant dose, catalyst dose, energy and intensity of radiation, stirring rate, temperature, and reaction time are affected by the degradation efficiency of photocatalyst for organic pollutants [17].

Here, the effect of extending the reaction time for the next 30 min for the photocatalytic degradation of MB dye using the rGO-CuO catalyst has been studied. When the reaction time was prolonged for 90 min for the degradation of the dye, the removal efficiency is increased to 92.8%, Figure 7c. The corresponding bathochromic shift in the intensity of the dye with time, Figure 7a,b as well as the pseudo-first-order reaction kinetics model parameters extracted from Figure 7d are also shown and results are tabulated in Table 2.

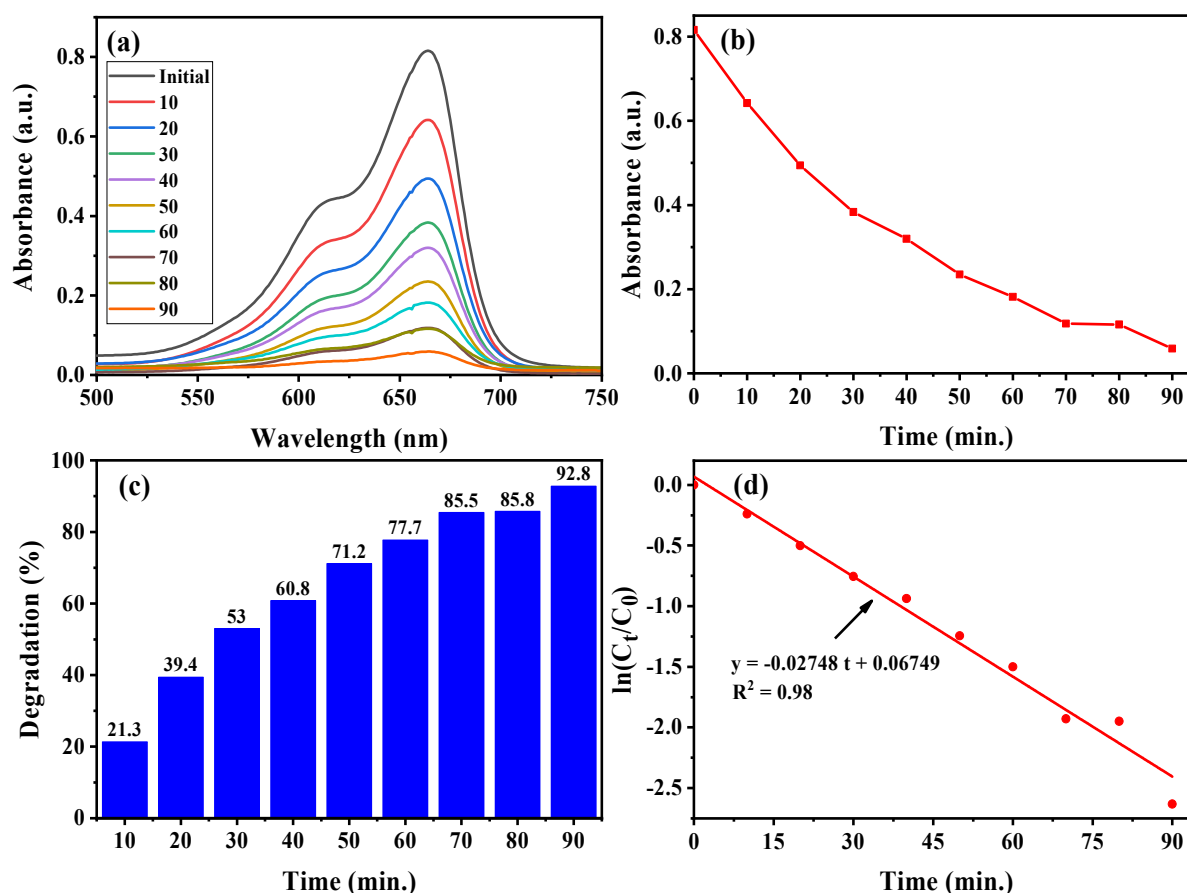


Figure 7. Change of absorbance with time (a,b), degradation achieved (c), and pseudo-first-order kinetics plot (d) for the degradation of MB under visible light for 90 min. using the synthesized rGO-CuO catalyst.

As discussed previously, the photocatalytic activity of rGO-CuO composites towards the degradation of MB and CR dyes are greater than bare CuO NPs. This could be attributed to the following possible reasons:

The charge transfer mechanism in rGO-CuO nanocomposites catalysts during the degradation process is illustrated in Figure 8. One possible reason for the enhanced activity of the nanocomposites are due to the electron-accepting property of rGO, which facilitates the efficient separation of e^-/h^+ pairs, resulting in more generations of radicals and an enhanced decomposition rate [39,40]. In addition, the enhanced degradation of MB could occur due to its high adsorption on the surface of the composite's particles, as the cationic dye molecules could easily form strong conjugation with the oxygen functional groups and the aromatic portion of the 2-D planar sheets in reduced GO, according to the studies reported earlier [41–43].

Another possible reason for rGO-CuO's catalytic effectiveness for the photocatalytic degradation of MB being more efficient than bare CuO could be due to sufficient electron transport between CuO and MB molecules. The electrons can then be transmitted by the conjugated graphene to the adsorbed MB molecules, causing the redox decomposition reaction. As MB can easily bind to rGO, the concentration of adsorbed MB molecules near CuO NPs in CuO/rGO composite will be larger than the concentration of bare CuO NPs, resulting in a faster catalytic breakdown rate.

Furthermore, during the excitation process, e^-/h^+ pairs are formed, the holes can be trapped by water or surface hydroxyls (single bond OH) to create the hydroxyl radical ($HO\cdot$), which is a powerful oxidizing agent for the breakdown of organic contaminants in wastewater [27]. Another likely enhancement of degradation of the dyes using the composites particles, as compared to bare CuO NPs, could be related to particle size [44,45].

Electrons can be transferred to the surface of the NPs, which then migrates to graphene. Thus, the recombination rate of e^-/h^+ pairs could be reduced as the size of the NPs lowers. The transport of electrons from graphene to molecules of methylene blue increased photocatalytic activity. Generally, the high catalytic activity of rGO/CuO nanocomposites for the degradation of MB could be attributed to a synergistic effect of methylene blue molecules' absorptivity on rGO, surface hydroxyl to produce HO^\cdot , the photocatalytic properties of CuO NPs, lower bandgap, and smaller particle size, all of which were achieved in a single synthetic process.

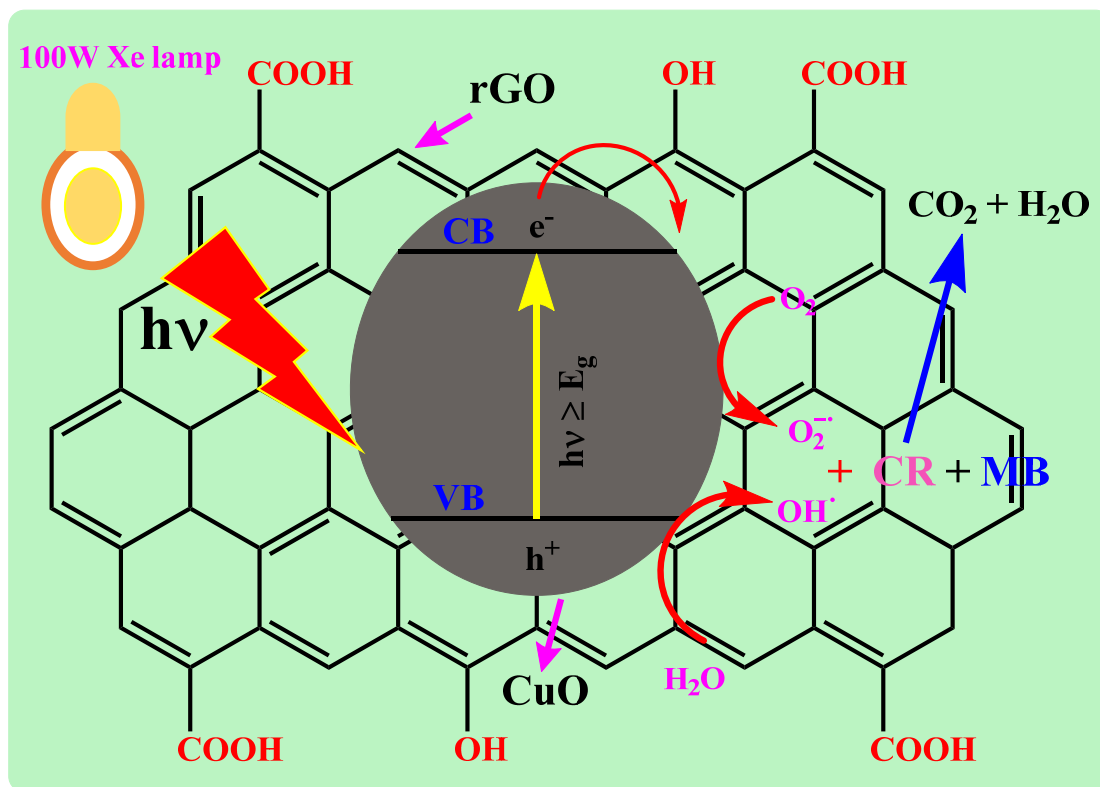


Figure 8. Formation of charge carriers and their transfer mechanism during the visible light assisted degradation of MB and CR dyes using rGO-CuO nanocomposites.

3. Experimental Section

3.1. Materials and Methods

All the chemicals used in this work were of analytical grade and used as such without further purification. The graphite powder (99.99%) and copper (II) nitrate trihydrate ($\text{Cu}(\text{NO}_3)_2 \cdot 3\text{H}_2\text{O}$, 99.9%), and 2-propanol were purchased from Sigma Aldrich.

3.2. Synthesis of CuO/rGO Nanocomposites

Exfoliation and oxidation of graphite powder were used for synthesizing GO using a modified Hummers and Offeman's method [11]. An impregnation approach combined with thermal treatment was used to produce CuO/rGO nanocomposites. The synthesis of CuO/rGO nanocomposite was carried out by $\text{Cu}(\text{NO}_3)_2 \cdot 3\text{H}_2\text{O}$ (0.13 g) and GO (0.3 g) were dissolved in 50 mL of 2-propanol and adjusting the pH level to 12. The resulting suspension was then sonicated for 30 min before being agitated with reflux at 83 °C for 3 h. Then, the suspension was centrifuged at 8000 rpm after being filtered with distilled water. Finally, the filtrate was freeze-dried and placed in a furnace at 400 °C for 30 min, producing CuO/rGO nanocomposite as the final product.

3.3. Instrumental Analysis

Powder X-ray diffraction (XRD) analysis was used to investigate the CuO/rGO nanocomposite, using CuK α radiation ($\lambda = 1.5406 \text{ \AA}$) and a quartz monochromator source (PANalytical X-ray diffractometer). For the functional group analysis, a single-beam Fourier-transform infrared (FT-IR) spectrometer (Model-Agilent, Cary 630 Spectrometer, JASCO International Co., Japan,) using the KBr pellet method was used to record the spectrum in the wavelength range of 4000 to 500 cm^{-1} . A Perkin-Elmer Lambda 650 spectrophotometer (PerkinElmer Inc., Singapore) was used to measure UV-Vis optical absorption. Field emission scanning electron microscope (FESEM) (JMS7500F, JEOL, Akishima, Japan) connected to the energy dispersive X-ray (EDX) detector were employed, respectively.

3.4. Photocatalytic Activity

The photocatalytic activity of the prepared CuO/rGO nanocomposite was tested for the degradation of MB and CR dyes taken separately. Firstly, 10 mg of CuO/rGO catalyst was immersed in 10 mL of distilled water, and the resulting suspension was stirred for 30 min in a dark room to establish adsorption/desorption equilibrium. After that, the suspension was added to a sealed round bottom flask containing 50 mL of $2.23 \times 10^{-5} \text{ M}$ aqueous solution of MB or CR dyes, and the catalytic reactions were performed at room temperature. The absorbance of the resulting supernatants was measured with a UV visible spectrophotometer, and the degree of decomposition of dyes was calculated using Equation (1).

4. Conclusions

An impregnation method, followed by a thermal treatment approach was used to synthesize rGO/CuO nanocomposites and tested by XRD, FTIR, UV-Vis, and SEM techniques. The prepared sample was analyzed for photocatalytic degradation of contaminant dyes, that is, MB and CR dyes, individually under visible light irradiation. This results in about 96% of decomposition for CR, while MB was degraded by nearly 78% in 1 h of illumination. The kinetics of the decomposition reactions can be satisfactorily described by a pseudo-first-order reaction model with reaction rate constants of 0.0459 and 0.0248 min^{-1} , respectively. The removal percentage of MB was further improved by prolonging the reaction time, and degradation of 93% was achieved in 90 min of irradiation. Additionally, the enhanced catalytic activity of rGO/CuO composites for the degradation of the dyes could be attributed to the good electron-accepting property of rGO in the composites, thereby promoting the efficiency of e^-/h^+ pairs separation and increasing rate of the degradation process. Further, the enhanced activity of the composites to the degradation of MB could be due to the better absorption of dye molecules on catalyst particles owing to the strong conjugation of an aromatic portion of the 2-D sheets and oxygen functional groups in rGO with dye molecules. Therefore, the synthesized rGO/CuO nanocomposites can be used in the dye degradation of organic pollutants in wastewater remediation.

Author Contributions: S.S.: Formal analysis, Conceptualization, methodology, Data curation, Validation and Original draft preparation. J.A.L.: Data curation, Visualization, and Validation. G.K.W.: Formal analysis, Investigation, Data curation, Visualization, and Validation. S.G.: Formal analysis, Data curation and Visualization. W.-C.O.: Funding acquisition. N.A.H.: Formal analysis, Visualization and Investigation. M.R.J.: Data curation, Visualization, and Validation. All authors have read and agreed to the published version of the manuscript.

Funding: This work was financially supported by University of Malaya Research Grant (RU001-2019, RU001-2020 and RU001-2021).

Data Availability Statement: All relevant data are within the paper.

Acknowledgments: The authors would like to acknowledge the University of Malaya.

Conflicts of Interest: The authors have no conflicts of interest to declare regarding the publication of this work.

References

1. Lignier, P.; Bellabarba, R.; Tooze, R.P. Scalable strategies for the synthesis of well-defined copper metal and oxide nanocrystals. *Chem. Soc. Rev.* **2012**, *41*, 1708–1720. [[CrossRef](#)] [[PubMed](#)]
2. Kumar, B.; Saha, S.; Ganguly, A.; Ganguli, A.K. A facile low temperature (350 C) synthesis of Cu₂O nanoparticles and their electrocatalytic and photocatalytic properties. *RSC Adv.* **2014**, *4*, 12043–12049. [[CrossRef](#)]
3. Kuo, C.-H.; Chen, C.-H.; Huang, M.H. Seed-Mediated Synthesis of Monodispersed Cu₂O Nanocubes with Five Different Size Ranges from 40 to 420 nm. *Adv. Funct. Mater.* **2007**, *17*, 3773–3780. [[CrossRef](#)]
4. Wang, D.B.; Yu, D.B.; Mo, M.S.; Liu, X.M.; Qian, Y.T. Seed-mediated growth approach to shape-controlled synthesis of Cu₂O particles. *J. Colloid Interf. Sci.* **2003**, *261*, 565–568. [[CrossRef](#)]
5. Zhang, H.; Lv, X.; Li, Y.; Wang, Y.; Li, J. P25-graphene composite as a high performance photocatalyst. *ACS Nano* **2010**, *4*, 380–386. [[CrossRef](#)] [[PubMed](#)]
6. Mun, D.-H.; Lee, H.J.; Bae, S.; Kim, T.-W.; Lee, S.H. Photocatalytic decomposition of graphene over a ZnO surface under UV irradiation. *Phys. Chem. Chem. Phys.* **2015**, *17*, 15683–15686. [[CrossRef](#)] [[PubMed](#)]
7. Zhang, Y.H.; Tang, Z.R.; Fu, X.Z.; Xu, Y.J. TiO₂–Graphene Nanocomposites for Gas-Phase Photocatalytic Degradation of Volatile Aromatic Pollutant: Is TiO₂–Graphene Truly Different from Other TiO₂–Carbon Composite Materials? *ACS Nano* **2010**, *4*, 7303–7314. [[CrossRef](#)] [[PubMed](#)]
8. Sathyamoorthy, R.; Mageshwari, K. Synthesis of hierarchical CuO microspheres: Photocatalytic and antibacterial activities. *Physical E* **2013**, *47*, 157–161. [[CrossRef](#)]
9. Zaman, S.; Zainelabdin, A.; Amin, G.; Nur, O.; Willander, M. Efficient catalytic effect of CuO nanostructures on the degradation of organic dyes. *J. Phys. Chem. Solids* **2012**, *73*, 1320–1325. [[CrossRef](#)]
10. Shaabani, B.; Alizadeh-Gheshlaghi, E.; Azizian-Kalandaragh, Y.; Khodayari, A. Preparation of CuO nanopowders and their catalytic activity in photodegradation of Rhodamine-B. *Adv. Powder Technol.* **2014**, *25*, 1043–1052. [[CrossRef](#)]
11. Lee, K.H.; Han, S.W.; Kwon, K.Y.; Park, J.B. Systematic analysis of palladium–graphene nanocomposites and their catalytic applications in Sonogashira reaction. *J. Colloid Interf. Sci.* **2013**, *403*, 127–133. [[CrossRef](#)]
12. Sun, Y.M.; Hu, X.L.; Luo, W.; Xia, F.F.; Huang, Y.H. Reconstruction of conformal nanoscale MnO on graphene as a high-capacity and long-life anode material for lithium ion batteries. *Adv. Funct. Mater.* **2013**, *23*, 2436–2444. [[CrossRef](#)]
13. Zeng, B.; Chen, X.; Luo, Y.; Liu, Q.; Zeng, W. Graphene spheres loaded urchin-like Cu_xO (x = 1 or 2) for use as a high performance photocatalyst. *Ceram. Int.* **2014**, *40*, 5055–5059. [[CrossRef](#)]
14. Zong, M.; Huang, Y.; Wu, H.; Zhao, Y.; Liu, P.; Wang, L. Facile preparation of RGO/Cu₂O/Cu composite and its excellent microwave absorption properties. *Mater. Lett.* **2013**, *109*, 112–115. [[CrossRef](#)]
15. Wang, M.; Huang, J.; Tong, Z.; Li, W.; Chen, J. Reduced graphene oxide–cuprous oxide composite via facial deposition for photocatalytic dye-degradation. *J. Alloys Compd.* **2013**, *568*, 26–35. [[CrossRef](#)]
16. Cheng, L.; Wang, Y.; Huang, D.; Tronganh, N.; Jiang, Y.; Yu, H.; Ding, N.; Ding, G.; Jiao, Z. Facile synthesis of size-tunable CuO/graphene composites and their high photocatalytic performance. *Mater. Res. Bull.* **2015**, *61*, 409–414. [[CrossRef](#)]
17. Weldegebräel, G.K. Synthesis method, antibacterial and photocatalytic activity of ZnO nanoparticles for azo dyes in wastewater treatment: A review. *Inorg. Chem. Commun.* **2020**, *120*, 108140. [[CrossRef](#)]
18. Weldegebräel, G.K. Photocatalytic and antibacterial activity of CuO nanoparticles biosynthesized using *Verbascum thapsus* leaves extract. *Optik* **2020**, *204*, 164230. [[CrossRef](#)]
19. Dhanalekshmi, S.B.; Priya, R.; Selvi, K.T.; Mangai, K.A.; Weldegebräel, G.K.; Garg, S.; Sagadevan, S. Microwave-assisted synthesis, characterization and photocatalytic activity of mercury vanadate nanoparticles. *Inorg. Chem. Commun.* **2021**, *131*, 108768. [[CrossRef](#)]
20. Chen, Q.W.; Zhang, L.Y.; Chen, G. Facile preparation of graphene-copper nanoparticle composite by in situ chemical reduction for electrochemical sensing of carbohydrates. *Anal. Chem.* **2012**, *84*, 171–178. [[CrossRef](#)]
21. Zhang, F.; Li, Y.; Gu, Y.-e.; Wang, Z.; Wang, C. One-pot solvothermal synthesis of a Cu₂O/Graphene nanocomposite and its application in an electrochemical sensor for dopamine. *Microchim. Acta* **2011**, *173*, 103–109. [[CrossRef](#)]
22. Shi, Y.; Qian, X.; Zhou, K.; Tang, Q.; Jiang, S.; Wang, B.; Wang, B.; Yu, B.; Hu, Y.; Yuen, R.K.K. CuO/graphene nanohybrids: Preparation and enhancement on thermal stability and smoke suppression of polypropylene. *Ind. Eng. Chem. Res.* **2013**, *52*, 13654–13660. [[CrossRef](#)]
23. Chen, W.; Fan, Z.; Lai, Z. Synthesis of core–shell heterostructured Cu/Cu₂O nanowires monitored by in situ XRD as efficient visible-light photocatalysts. *J. Mater. Chem. A* **2013**, *1*, 13862–13868. [[CrossRef](#)]
24. Xu, C.; Wang, X.; Yang, L.; Wu, Y. Fabrication of a graphene–cuprous oxide composite. *J. Solid State Chem.* **2009**, *182*, 2486–2490. [[CrossRef](#)]
25. Sagadevan, S.; Chowdhury, Z.Z.; Johan, M.R.; Aziz, F.A.; Salleh, E.M.; Hawa, A.; Rafque, R.F. A one-step facile route synthesis of copper oxide/reduced graphene oxide nanocomposite for supercapacitor applications. *J. Exp. Nanosci.* **2018**, *13*, 284–296. [[CrossRef](#)]
26. Nafey, A.; Addad, A.; Sieber, B.; Chastanet, G.; Barras, A.; Szunerits, S.; Boukherroub, R. Reduced graphene oxide decorated with Co₃O₄ nanoparticles (rGO-Co₃O₄) nanocomposite: A reusable catalyst for highly efficient reduction of 4-nitrophenol, and Cr(VI) and dye removal from aqueous solutions. *Chem. Eng. J.* **2017**, *322*, 375–384. [[CrossRef](#)]

27. Dutta, S.; Das, K.; Chakrabarti, K.; Jana, D.; De, S.; De, S. Highly efficient photocatalytic activity of CuO quantum dot decorated rGO nanocomposites. *J. Phys. D* **2016**, *49*, 315107. [[CrossRef](#)]
28. Alves, D.C.; Silva, R.; Voiry, D.; Asefa, T.; Chhowalla, M. Copper nanoparticles stabilized by reduced graphene oxide for CO₂ reduction reaction. *Mater. Renew. Sustain. Energy* **2015**, *4*, 1–7. [[CrossRef](#)]
29. Paredes, J.I.; Villar-Rodil, S.; Martínez-Alonso, A.; Tascón, J.M.D. Graphene oxide dispersions in organic solvents. *Langmuir* **2008**, *24*, 10560–10564. [[CrossRef](#)] [[PubMed](#)]
30. Fernández-Merino, M.J.; Guardia, L.; Paredes, J.; Villar-Rodil, S.; Solís-Fernández, P.; Martínez-Alonso, A.; Tascón, J. Vitamin C is an ideal substitute for hydrazine in the reduction of graphene oxide suspensions. *J. Phys. Chem. C* **2010**, *114*, 6426–6432. [[CrossRef](#)]
31. Hou, S.; Su, S.; Kasner, M.L.; Shah, P.; Patel, K.; Madarang, C.J. Formation of highly stable dispersions of silane-functionalized reduced graphene oxide. *Chem. Phys. Lett.* **2010**, *501*, 68–74. [[CrossRef](#)]
32. Kumar, S.; Ojha, A.K.; Bhorolua, D.; Das, J.; Kumar, A.; Hazarika, A. Facile synthesis of CuO nanowires and Cu₂O nanospheres grown on rGO surface and exploiting its photocatalytic, antibacterial and supercapacitive properties. *Phys. B Condens. Matter* **2019**, *558*, 74–81. [[CrossRef](#)]
33. Mousset, E.; Oturan, N.; Oturan, M.A. An unprecedented route of OH radical reactivity evidenced by an electrocatalytic process: Ipso-substitution with perhalogenocarbon compounds. *Appl. Catal. B Environ.* **2018**, *226*, 135–146. [[CrossRef](#)]
34. Botsa, S.M.; Basavaiah, K. Removal of Nitrophenols from wastewater by monoclinic CuO/RGO nanocomposite. *Nanotechnol. Environ. Eng.* **2018**, *4*, 1–7. [[CrossRef](#)]
35. Siddique, S.; Zain-ul-Abdin; Waseem, M.; Naseem, T.; Bibi, A.; Hafeez, M.; Din, S.U.; Haq, S.; Qureshi, S. Photo-Catalytic and Anti-microbial Activities of rGO/CuO Nanocomposite. *J. Inorg. Organomet. Polym. Mater.* **2021**, *31*, 1359–1372. [[CrossRef](#)]
36. Ravi, K.; Mohan, B.S.; Sree, G.S.; Raju, I.M.; Basavaiah, K.; Rao, B.V. ZnO/RGO nanocomposite via hydrothermal route for photocatalytic degradation of dyes in presence of visible light. *Int. J. Chem. Stud.* **2018**, *6*, 20–26.
37. Aragaw, B.A.; Dagnaw, A. Copper/reduced graphene oxide nanocomposite for high performance photocatalytic methylene blue dye degradation. *Ethiop. J. Sci. Technol.* **2019**, *12*, 125–137. [[CrossRef](#)]
38. Ajmal, A.; Majeed, I.; Malik, R.N.; Idriss, H.; Nadeem, M.A. Principles and mechanisms of photocatalytic dye degradation on TiO₂ based photocatalysts: A comparative overview. *RSC Adv.* **2014**, *4*, 37003–37026. [[CrossRef](#)]
39. Li, B.; Liu, T.; Hu, L.; Wang, Y. A facile one-pot synthesis of Cu₂O/RGO nanocomposite for removal of organic pollutant. *J. Phys. Chem. Solids* **2013**, *74*, 635–640. [[CrossRef](#)]
40. Ramesha, G.K.; Kumara, A.V.; Muralidhara, H.B.; Sampath, S. Graphene and graphene oxide as effective adsorbents toward anionic and cationic dyes. *J. Colloid Interf. Sci.* **2011**, *361*, 270–277. [[CrossRef](#)] [[PubMed](#)]
41. Yang, S.-T.; Chen, S.; Chang, Y.; Cao, A.; Liu, Y.; Wang, H. Removal of methylene blue from aqueous solution by graphene oxide. *J. Colloid Interf. Sci.* **2011**, *359*, 24–29. [[CrossRef](#)] [[PubMed](#)]
42. Liu, T.; Li, Y.; Du, Q.; Sun, J.; Jiao, Y.; Yang, G.; Wang, Z.; Xia, Y.; Zhang, W.; Wang, K.; et al. Adsorption of methylene blue from aqueous solution by graphene. *Colloid. Surf. B* **2012**, *90*, 197–203. [[CrossRef](#)] [[PubMed](#)]
43. Sagadevan, S.; Lett, J.A.; Weldegebriela, G.K.; Oh, W.C.; Alshahateet, S.F.; Fatimah, I.; Fatimah, I.; Mohammad, F.; Al-Lohedan, H.A.; Paiman, S.; et al. Enhanced gas sensing and photocatalytic activity of reduced graphene oxide loaded TiO₂ nanoparticles. *Chem. Phys. Lett.* **2021**, *780*, 138897. [[CrossRef](#)]
44. Li, Y.; Yang, X.-Y.; Rooke, J.; van Tendeloo, G.; Su, B.-L. Ultralong Cu(OH)₂ and CuO nanowire bundles: PEG200-directed crystal growth for enhanced photocatalytic performance. *J. Colloid Interf. Sci.* **2010**, *348*, 303–312. [[CrossRef](#)] [[PubMed](#)]
45. Hagfeldt, A.; Gratzel, M. Light-induced redox reactions in nanocrystalline systems. *Chem. Rev.* **1995**, *95*, 49–68. [[CrossRef](#)]